Simulating medical applications of tissue optical property and shape imaging using open-source ray tracing software

J. Crowley[a] and G.S.D. Gordon[a]

[a]Faculty of Engineering, The University of Nottingham, Nottingham, United Kingdom

ABSTRACT

Oesophageal cancer and colon cancer have five year survival rates of 15%[1] and 63%[2] respectively. These low survival rates are due in part to poor early detection during endoscopic screening, with conventional endoscopes providing insufficient information about tissue properties to spot a wide range of potential tumours. Improving early detection of gastrointestinal cancers would dramatically increase their five year survival rates. Spatial Frequency Domain Imaging (SFDI) is a low-cost imaging technique that can measure absorption, scattering and shape as potential indicators of cancer. Specific absorption and scattering properties are known to be linked to malignancy in the oesophagus,[3] and shape is an important indicator in colon cancer.[4] Though a range of research and commercial SFDI systems have been developed,[5] adapting these for *in vivo* clinical application is challenging due to constraints imposed by miniaturisation, sample geometry and illumination conditions. To facilitate design of novel SFDI systems under such constraints, we have developed a model of an SFDI imaging system built on the open-source 3D modelling software *Blender*. Using Blender's Cycles ray-tracing engine, we are able to simulate a range of different scattering and absorption coefficients for a number of different imaging configurations, sample geometries and illumination patterns. Using established processing algorithms, we show we can recover maps of absorption, scattering and shape in a range of simulated *ex vivo* and *in vivo* imaging geometries with relevance to clinical detection of tumours. Our system enables accessible exploration of different optical configurations and realistic illumination conditions that will inform future design of compact, low-cost instruments.

Keywords: Spatial frequency domain imaging, Fourier transform profilometry, oesophageal cancer, colon cancer, optical properties, low-cost

1. INTRODUCTION

1.1 Spatial frequency domain imaging

Spatial Frequency Domain Imaging is a well-established technique in biomedical imaging with numerous research[6,7] and commercial systems now available.[8] By performing SFDI at several different wavelengths, maps of tissue oxyhaemoglobin and deoxyhaemoglobin can be calculated from the resulting absorption maps.[9] This is useful for surgeons reattaching blood vessels to transplanted organs. SFDI has also been shown to provide tissue oxygenation measurements of blocked blood vessels comparable to measurements by FDA approved devices.[10] Another application is in the imaging of skin burns. SFDI has been shown to accurately detect burn depth,[11] and SFDI derived tissue characteristics such as tissue haemoglobin and oxygen saturation have been shown to monitor burn progression.[12] Such quantitative information at early stages could better inform treatment decisions compared to more subjective indicators currently used. SFDI can also be used in oncology to detect tumour margins, by improving contrast between normal tissue and invasive cancer.[13]

Imaging in the spatial frequency domain consists of projecting a known 2D illumination pattern onto a sample and examining the amplitude of the reflected/transmitted illumination patterns' amplitude as a function of spatial frequency. Sinusoidal patterns of known spatial frequency are typically used as the illumination pattern (see Fig. 1), although recent work has drawn on the field of compressed sensing to show that randomised speckle

Further author information: (Send correspondence to J.C.)
J.C.: E-mail: jane.crowley@nottingham.ac.uk
G.S.D.G.: E-mail: george.gordon@nottingham.ac.uk

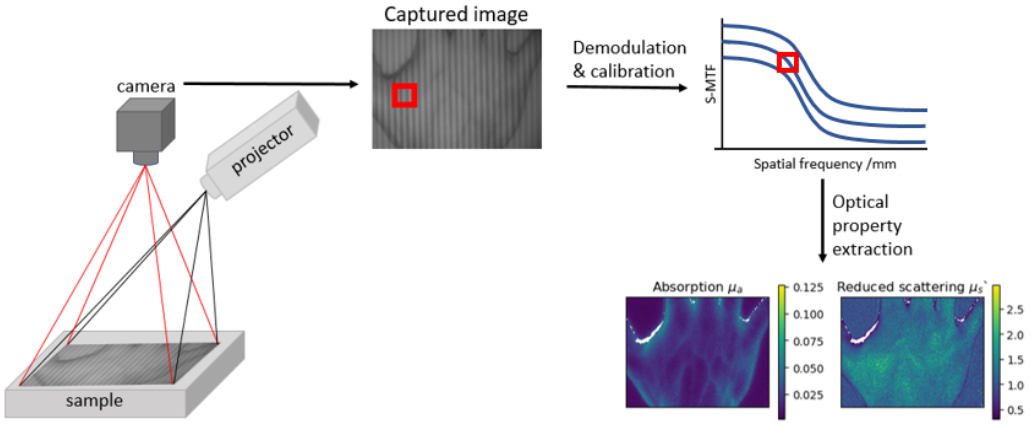

Figure 1: Typical SFDI apparatus uses a projector to illuminate a sample with sinusoidal patterns, which are then captured with a camera. Demodulation of these images and comparison with reference models of absorption and scattering can then produce 2D maps of these properties. (Captured image taken from[5])

patterns can also be used.[14] In this way, SFDI can be viewed as a special case of more general structured illumination techniques.[15] These sinusoids are often projected onto the sample at small angle from the normal (e.g. 4°) to minimise specular reflection recorded by the camera.[6] This has the added advantage of enabling fringe profilometry if a telecentric lens configuration is used.[16]

This incident light is then scattered or absorbed by the sample, which modifies the amplitude of the sinusoid in a way that depends on spatial frequency. An image of the sinusoid, having been modified by the tissue, is captured with a camera typically oriented orthogonally to the sample. Captured images are then processed to determine the *modulation index* of the reflected sinusoid at two or more spatial frequencies. This can be achieved with only a single such image by using Fourier-domain filtering to separate out an AC and DC component, a technique termed Single Snapshot of Optical Properties (SSOP),[17] but more commonly the sinusoidal pattern is phase-shifted (0°, 120° and 240°) at 2 different AC frequencies producing 6 or more images.[18] Next, the modulation properties of a reference phantom with known optical properties are used to correct for the *modulation transfer function (MTF)* of the imaging system at each spatial frequency, allowing the diffuse reflectance values of the sample to be estimated accurately. Using these diffuse reflectance values, the absorption and scattering properties of a sample can be determined using a look up table (LUT) generated by solving the diffusion equations for light propagation in scattering and absorbing media or via Monte-Carlo simulation.[19]

Currently, a number of open source software packages relevant to SFDI exist. *AppSFDI*[20] can perform demodulation from a set of images taken at spatial frequencies of 0 and 0.2 mm^{-1}. It can also produce maps of absorption and reduced scattering if images of a reference phantom of known optical properties are also given. There is also a software available for using deep learning to perform the demodulation and production of absorption and scattering maps.[21] However, perhaps of more relevance to this is work is software that simulates the optical behaviour of materials under conditions of scattering and absorption. *Toast++*[22] is widely used for forward and inverse modelling in diffuse optical tomography. However, because the software is designed for diffuse optical tomography, it typically simulates a small number of sources and detectors placed on the surface of sample. It is thus less well-suited to considering the effects of complex illumination patterns and very high-resolution detectors placed some distance away from the sample, as is required for SFDI. Recently, a new software package, *ValoMC*, was released that can perform Monte Carlo simulations of light in tissue for large samples,[23] and there are numerous other more specialised pieces of Monte-Carlo simulation software such as *OptogenSIM*[24] and *FullMonte*.[25] However, all of these packages typically require meshes to be defined in another package, and do not fully consider lighting conditions, camera positions, or realistic projection of complex structured illumination. This makes it difficult to use them to design practical SFDI systems. Currently, such systems are typically designed experimentally and require testing with, for example, numerous complex phantoms shapes.[26]

1.2 Fringe Profilometry

In addition to measuring optical absorption and scattering, structured illumination can also provide 3D depth information about a sample. Structured light has been successfully used for shape detection with application to sizing colon polyps.[27] In diagnosing gastrointestinal cancers, the size and shapes of polyps is important in identifying the risk of cancer and in the decision making process of the polyps resection.[4] The current decision making process is subjective and the risk of the majority of lesions is overestimated. However, shape detection via structured light is currently much more widely used in industrial inspection applications and consequently there are numerous commercial systems available.[28,29]

One well-established technique for this is Fourier Transform Profilometry (FTP), sometimes called Moire profilometry, in which either a sinusoidal or Ronchi grating is projected onto a $3D$ object, which is then imaged.[30] Based on a single such image, spatial frequency domain processing can then be applied to determine the shape of the object, which can be achieved in near-real time. The height can be calculated by knowing the distance from reference plane to projector, l_0, the camera-projector distance d, and the projected spatial frequency f_0:

$$h(x,y) = \frac{\Delta\phi(x,y) l_0}{\Delta\phi(x,y) - d2\pi f_0} \tag{1}$$

where $\Delta\phi(x,y)$ is the phase modulation relative to the flat reference image caused by the shift in height. In order to work, this method requires a small angle of projection relative to camera to create this phase shift and also requires approximate telecentricity of illumination optics to avoid frequency shifts of the structured pattern.[31]

There is freely-available software for both recovery of phase maps from profilometry images (*PhaseWare*[32]) and also for simulation of fringe projection onto objects.[33,34] However, these typically assume purely reflecting objects and do not consider more complex materials with scattering and absorption properties.

2. METHODS

2.1 Blender ray tracing set up

We show here, for the first time, that it is possible to perform both SFDI and fringe profilometry with realistic sample and image geometries using freely available ray-tracing software. Specifically, we use open source computer graphics software Blender *(v 2.82a)* to simulate an imaging system consisting of a projector, a camera, and an object to be imaged with customizable material properties. An example set-up for imaging a planar object is shown in Fig. 2. Blender comes with a full ray tracing engine called *Cycles* that can simulate scattering and absorbing material. The numerical simulation of many rays being randomly transmitted, reflected or scattered is in many respects similar to Monte-Carlo approaches.

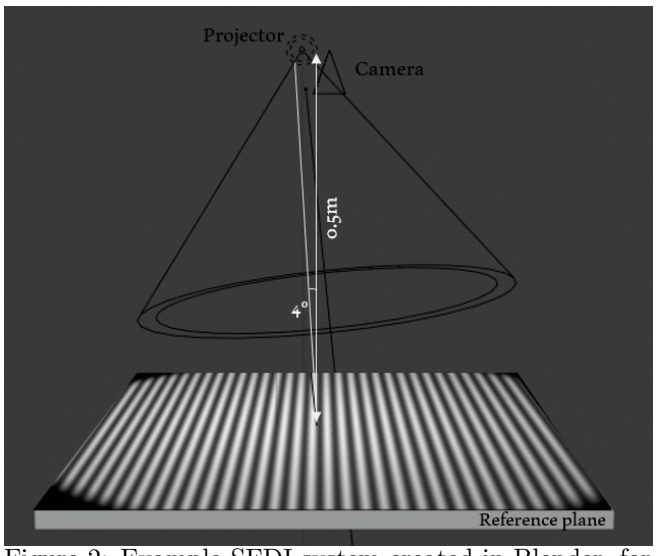

Figure 2: Example SFDI system created in Blender, for measuring a planar sample.

Here, we use a spotlight illumination with a power of 3W for the illumination source. The projection is always in focus but grows larger with distance – the assumption of telecentricity is therefore only valid for objects of relatively small height compare to the cone of projection. However, this height limit can easily be increased by reducing the projector's spot size (or solid-angle). A perspective-projection camera with a focal length of 50mm is used, though Blender also supports other projection paradigms such as orthographic projection that may be useful in other geometries (e.g. fish-eye lenses). However, the perspective camera closely approximates most real-world cameras. The projector and camera are positioned on the same plane, with the

projector at a 4° angle to the camera. The camera is positioned orthogonal to the imaging plane, at a distance of 0.5m. This offset in angle limits the coupling of specularly reflected light, especially for planar samples.

Materials in Blender are defined using pre-built shaders that can be combined together using a node system. Scattering is simulated by mixing two shaders together – subsurface scattering and transparent bi-directional scattering distribution function (BSDF). Subsurface scattering simulates light penetrating the surface of the material and bouncing around until it either escapes or is absorbed. The transparent BSDF adds transparency to the material without adding any refraction – this is ensured by matching the refractive index. A weight factor from 0 to 1 is used to mix the two shaders, with the weights of each constrained to sum to 1. A scattering factor of 0 represents, in this case, the material being entirely transparent. Similarly, a scattering factor of 1 represents the material properties being entirely due to subsurface scattering. The subsurface scattering material has a scattering radius and scale properties that are adjusted in advance such that the total scattering is very high, which then represents the maximum scattering that can be achieved by this mixing approach. The reason this mixing approach is used, rather than simply changing the radius of scattering, is because reducing the scattering radius to zero creates a specularly reflecting object, rather than a transparent object (i.e. no scattering) as is required.

Absorption is implemented using a custom material simulating transmissivity of light through the material, calculated from the Lambert Beer Law:[35]

$$T = \frac{I}{I_0} = e^{-\mu_a L} \tag{2}$$

where I and I_0 are the transmitted and incident light respectively, L is the path length of light travelled and μ_a is the absorption coefficient of the material, which is set to 1 mm^{-1}.

The composite material is a weighted mix of the scattering material and the absorbing material, where a factor of 0 represents a purely absorbing material and a factor of 1 represents a purely scattering material. Therefore, to alter the material's properties there are two parameters which can be altered; scattering factor and final factor.

Next, we must relate real-world optical properties to the system's two variable factors. To do this, we estimated the diffuse reflectance of imaged sinusoidal patterns projected at spatial frequencies ranging from $0 - 0.135$ mm^{-1} for a range of factor values. For each spatial frequency and set of factors, SFDI was carried out to extract the diffuse reflectance. This requires the use of a 'reference sample' to account for the system MTF. Here, the reference modulation amplitude image used was a purely scattering material, which serves an arbitrary reference. By comparison with curves from literature (in particular Cuccia et al.[18]) we can then calibrate these curves to match, so that the scattering and final factors can produce known reduced scattering and absorption coefficients.

For this initial proof-of-principle, we examine only absorption and scattering. However, we note that Blender offers a wide range of additional options that could extend this in future. For example, anisotropy can be specified to enable preferential forward or backward scattering, refractive index can be changed to examine the impact of specular reflection, scattering can have different length scales for red, green and blue channels offering some wavelength dependent behaviour. In addition to this, materials can have different colours, or there can be stray background light or water layers on samples to mimic realistic behaviour. Further, Blender can also produce time-dependent behaviour, e.g. movement, change of properties, that could be used to simulate realistic conditions. We intend to explore this parameter space in future.

We next implemented the algorithm presented in[18] to reconstruct optical property maps. We imaged both flat samples, tumour-like samples, and also samples with a hollow cylindrical geometry to mimic the gastrointestinal tract. Further, we also tested illumination using different patterns tailored to a cylindrical geometry and mimicking speckle pattern illumination.

To test shape measurement using fringe profilometry we introduced some specular reflection from the sample surface in order for a proof-of-principle. This is in line with previous studies that have shown typical tissue samples have sufficient specular reflection to enable both SFDI and profilometry simultaneously.[16]

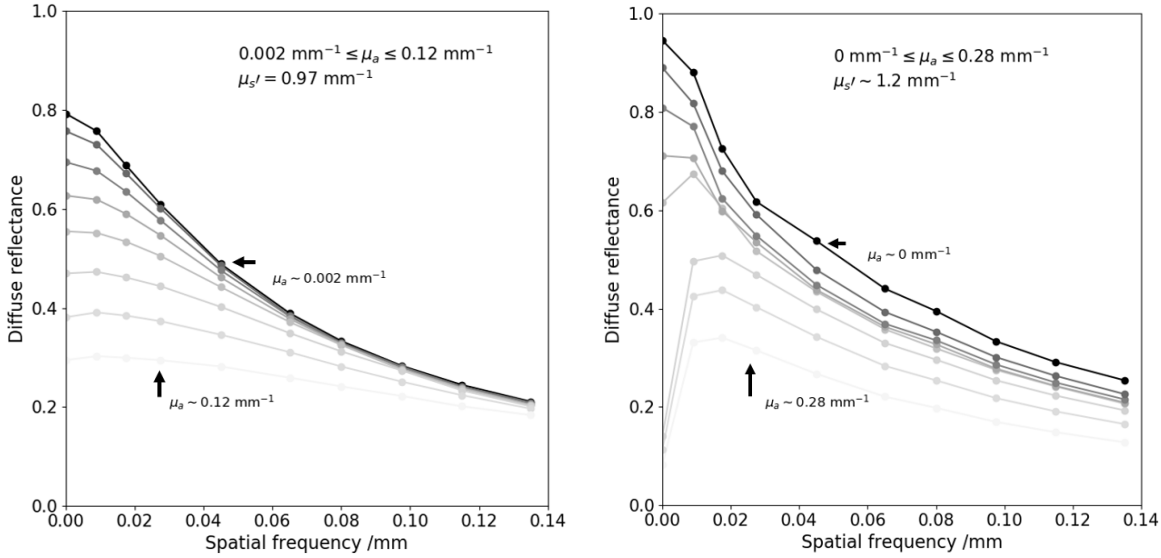

(a) (b)

Figure 3: (a) Diffuse reflectance vs spatial frequency curve adapted from[18] showing the effect of changing scattering coefficient. (b) Diffuse reflectance vs spatial frequency for varying scattering factor values in our Blender model. Scattering and absorption coefficients are determined by calibration against curves from (a), but cover a wider range due to our choice of 'maximally scattering' material. Overall, we find good agreement between the shapes and are thus able to relate our scattering factor and final factor with reduced scattering and absorption.

3. RESULTS

In order to calibrate the system, it was necessary to relate the varying factor values to absorption and reduced scattering coefficients. To do this, the average diffuse reflectance value of a sample for varying scattering factor values was recorded at multiple spatial frequencies. The points in Fig 3b, represent the average diffuse reflectance value over the entire image. To obtain these values, the diffuse reflectance values of the maximum and minimum curves in Fig 3a for a specific spatial frequency were recorded. Images of the material at varying final factor and scattering factor values were obtained at this specific spatial frequency, and their diffuse reflectance values calculated. The diffuse reflectance values were calibrated arbitrarily to a reference phantom of final factor of 1 and scattering factor of 1, with $\mu_a = 0$ mm^{-1} and $\mu_s' = 1.5$ mm^{-1}. Then, the diffuse reflectance values of maximum and minimum curves at a specific spatial frequency from Fig 3a could be matched to specific final factor and scattering factor values. We found that keeping final factor constant at 0.9 gave the largest range of values for varying the scattering factor. By varying the scattering factor between $0.005 - 0.89$ (the two values which were empirically determined to span the curves from Fig 3a) over the spatial frequency range $0 - 0.135$ mm^{-1}, we were able to produce curves shown in Fig 3b. Therefore, diffuse reflectance values were obtained against a simulated reference phantom of $\mu_a = 0$ mm^{-1} and $\mu_s' = 1.5$ mm^{-1} as it was found these values gave curves of most similar shape to Fig 3a. The optical properties of Fig 3b were calculated via a look up table in *Python* code.

Having verified simulation of absorption and scattering material, we next demonstrate the ease with which sample geometries can be varied. To do this, we created a spheroidal object with several spheroidal abnormalities, shown in Fig 4, to mimic a tumour. As shown by *Holmer et. al.*,[36] in the wavelength range of visible light, the absorption and reduced scattering coefficients of adenocarcinoma and squamous cell carcinoma (tumour tissue) are broadly lower than healthy stomach and oesophageal tissue. Appropriate optical properties were chosen, using the graph in Fig 3 to determine factor settings, so that the flat background mimicked healthy tissue, and the raised spheroid object, mimicked cancerous tissue. The optical property coefficients chosen were $\mu_a = 0.142$ mm^{-1} and $\mu_s' = 1.49$ mm^{-1} for the background, healthy tissue and $\mu_a = 0.015$ mm^{-1} and $\mu_s' = 1.27$ mm^{-1} for

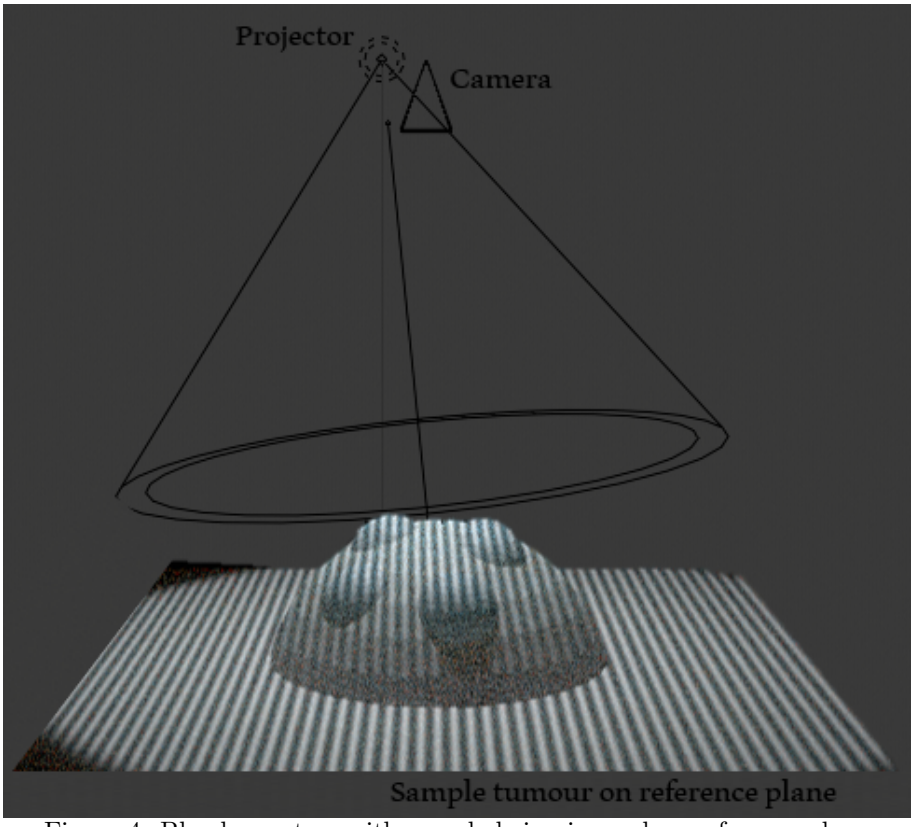

Figure 4: Blender system with sample being imaged on reference plane

cancerous tissue. A 2D Gaussian filter was applied to the absorption and reduced scattering coefficient maps in Fig 5c and 5d to reduce noise.

The lower absorption value can be clearly seen in Fig 5c. The plotted values for the reduced scattering coefficient of background healthy tissue and spheroid in Fig 5d are slightly lower than the expected values. This is in part due to calibration error, and a more iterative calibration approach is required to deliver more accurate results. Notably, the contrast provided by these optical property maps is visually improved compared to a conventional image, shown in Fig 5a, which illustrates the clinically relevant contrast improvement that SFDI can offer.

We performed a 3D shape reconstruction using Fourier transform profilometry, as shown in Figure 5b. The height of the spheroid was simulated to be 110 mm, representing a large tumour. Fig 5b shows that this height was successfully reconstructed.

We show the flexibility of our Blender system to enable more complex geometries and illumination profiles. First, we show illumination down a tube, designed to mimic the gastrointestinal tract, using a standard sinusoidal pattern (see Fig 6a). This shows how the pattern is distorted when projected down a tube, which would in practice result in non-uniform spatial frequencies on the sample. Based on simple reverse projections from this pattern, we developed a projection pattern of concentric circles of decreasing radius that creates a more uniform spatial frequency distribution when incident on the tube walls (Fig. 6b). This capability will allow us to test different illumination patterns before physically constructing such a system. Further, we can also examine the relative intensity along the tube length and correct for this when reconstructing diffuse reflectance.

Finally, we show for our tumour sample that it can be illuminated using a laser speckle pattern (Fig 7b), to simulate recent experimental work.[14] This technique, called speckle illumination spatial frequency domain imaging (si-SFDI) works by sampling the modulation transfer function of the imaged sample at a known spatial frequency. By calibrating with a phantom of known optical properties, changes in the MTF determine the optical

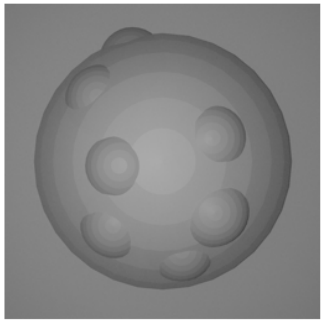

(a)

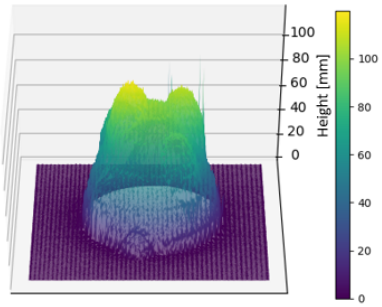

(b)

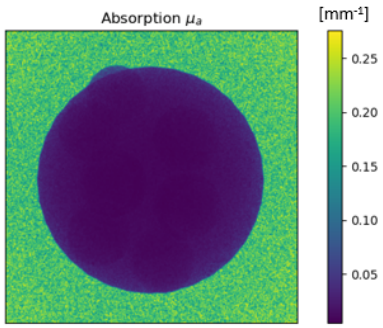

(c)

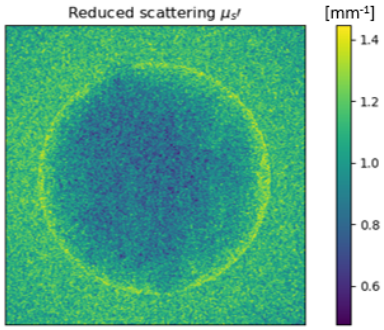

(d)

Figure 5: A simulated spheroidal tumour phantom on flat homogeneous background: (a) Conventional image of simulated tumour, (b) 3D profile of simulated tumour reconstructed via FTP, (c) Map of absorption coefficient of simulated tumour showing contrast compared to healthy tissue background, (d) Map of reduced scattering coefficient of simulated tumour showing contrast compared to healthy tissue background.

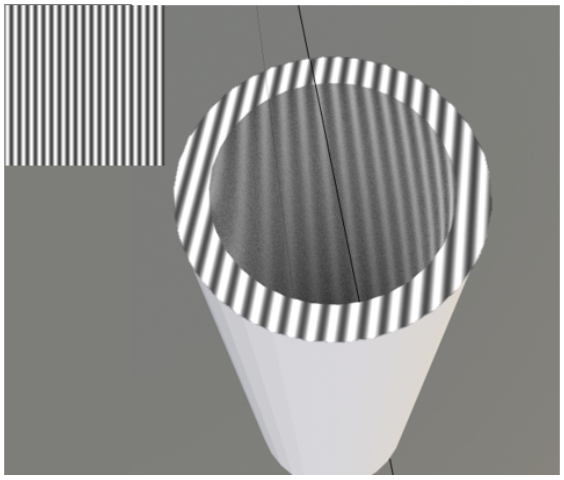

(a)

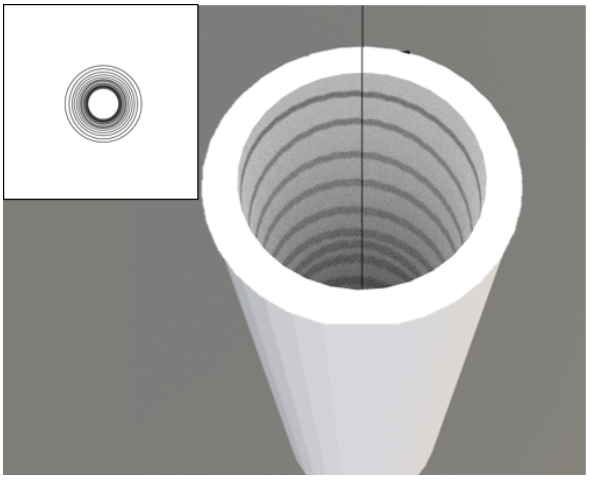

(b)

Figure 6: Illumination patterns projected down a tube designed to mimic the gastrointestinal tract: (a) Conventional sinusoidal pattern, (b) Concentric circles pattern

properties of the sample. This technique is desirable in geometries such as that presented in endoscopy because speckle patterns are generated over a large field of view with a basic illumination source.

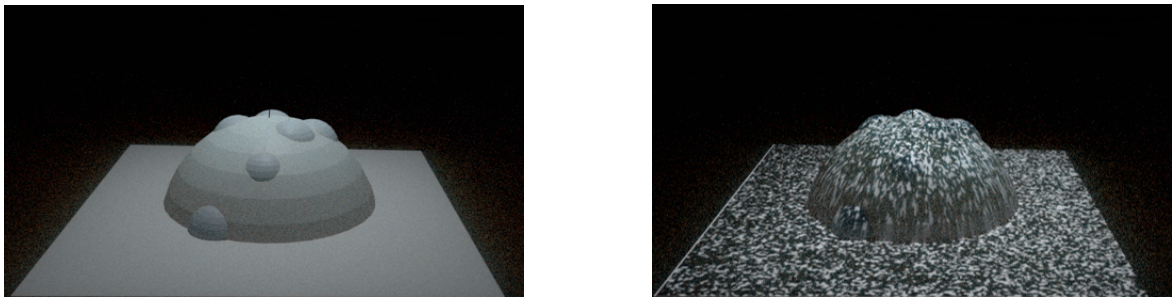

(a) (b)

Figure 7: Comparison of uniform projection and speckle pattern projection on simulated tumour: (a) Conventional uniform pattern projected onto tumour sample, (b) Speckle pattern projected onto tumour sample.

4. DISCUSSION

We have presented an SFDI simulation system that uses the open source Blender computer graphics software to enable creation of objects with a range of calibrated reduced scattering and absorption coefficients, complex object and imaging geometries, projection of arbitrary illumination patterns, and simultaneously reconstruction of 3D shape using fringe profilometry.

Though this work presents an important first proof-of-principle, there are many improvements yet to be explored. This includes more accurate calibration with data from literature, use of advanced material properties such as anisotropic scattering, different refractive index, wavelength dependence – all of which Blender can implement. Blender's Python scripting function could in future be used to automate calibration processes, or enable optimisation of system parameters to maximise signal-to-noise in recovered optical property maps.

We foresee many future applications of this work, one of which is the testing of different illumination sources. This could be used to help further miniaturise ultra-compact low-cost SFDI systems,[37] and enable them to make use of non-standard illumination patterns, e.g. from an LED array, or to use lower resolution cameras. Testing these effects in software may therefore rapidly accelerate the design process.

ACKNOWLEDGMENTS

GSDG would like to acknowledge a UKRI Future Leaders Fellowship (MR/T041951/1) and a UNICAS Award from the University of Nottingham. The authors would like to thank Samuel Powell for his helpful discussions and insights.

REFERENCES

[1] CRUK, "Oesophageal Cancer Statistics," (4 2020).

[2] Cancer.net, "Colon Cancer Statistics," (6 2020).

[3] Douplik, A., Zanati, S., Saiko, G., Streutker, C., Loshchenov, M., Adler, D., Cho, S., Chen, D., Cirocco, M., Marcon, N., Fengler, J., and Wilson, B. C., "Diffuse reflectance spectroscopy in Barrett's Esophagus: Developing a large field-of-view screening method discriminating dysplasia from metaplasia," *Journal of Biophotonics* **7**(5), 304–311 (2014).

[4] Burgess, N. G., Hourigan, L. F., Zanati, S. A., Brown, G. J., Singh, R., Williams, S. J., Raftopoulos, S. C., Ormonde, D., Moss, A., Byth, K., Mahajan, H., McLeod, D., and Bourke, M. J., "Risk Stratification for Covert Invasive Cancer Among Patients Referred for Colonic Endoscopic Mucosal Resection: A Large Multicenter Cohort," *Gastroenterology* **153**(3), 732–742 (2017).

[5] Applegate, M. B., Jr, J. P. A., Tabassum, S. M., Tilbury, K., Saager, R. B., Roblyer, D., Applegate, M. B., Karrobi, K., Jr, J. P. A., Austin, W., Tabassum, S. M., Aguénounon, E., Tilbury, K., Saager, R. B., Gioux, S., and Roblyer, D., "OpenSFDI : an open-source guide for constructing a spatial frequency domain imaging system," **25**(1) (2020).

[6] Cuccia, D. J., Bevilacqua, F., Durkin, A. J., and Tromberg, B. J., "Modulated imaging: quantitative analysis and tomography of turbid media in the spatial-frequency domain," *Optics Letters* **30**(11), 1354 (2005).

[7] Gioux, S., Mazhar, A., and Cuccia, D. J., "Spatial frequency domain imaging in 2019: principles, applications, and perspectives," *Journal of Biomedical Optics* **24**, 1 (6 2019).

[8] "Spatial frequency domain imaging, https://modulim.com/technology/sfdi/."

[9] Chen, M. T. and Durr, N. J., "Rapid tissue oxygenation mapping from snapshot structured-light images with adversarial deep learning," *arXiv* **25**(November), 1–12 (2020).

[10] Gioux, S., Mazhar, A., Lee, B. T., Lin, S. J., Tobias, A. M., Cuccia, D. J., Stockdale, A., Oketokoun, R., Ashitate, Y., Kelly, E., Weinmann, M., Durr, N. J., Moffitt, L. A., Durkin, A. J., Tromberg, B. J., and Frangioni, J. V., "First-in-human pilot study of a spatial frequency domain oxygenation imaging system," *Journal of Biomedical Optics* **16**(8), 086015 (2011).

[11] Mazhar, A., Saggese, S., Pollins, A. C., Cardwell, N. L., Nanney, L., and Cuccia, D. J., "Noncontact imaging of burn depth and extent in a porcine model using spatial frequency domain imaging,"

[12] Ponticorvo, A., Burmeister, D. M., Yang, B., Choi, B., Christy, R. J., and Durkin, A. J., "Quantitative assessment of graded burn wounds in a porcine model using spatial frequency domain imaging (SFDI) and laser speckle imaging (LSI)," *Biomedical Optics Express* **5**, 3467 (10 2014).

[13] Laughney, A. M., Krishnaswamy, V., Rice, T. B., Cuccia, D. J., Barth, R. J., Tromberg, B. J., Paulsen, K. D., Pogue, B. W., and Wells, W. A., "System analysis of spatial frequency domain imaging for quantitative mapping of surgically resected breast tissues," *Journal of Biomedical Optics* **18**, 036012 (3 2013).

[14] Chen, M. T., Papadakis, M., and Durr, N. J., "Speckle illumination SFDI for projector-free optical property mapping," *Optics Letters* **46**, 673 (2 2021).

[15] Ströhl, F. and Kaminski, C. F., "Frontiers in structured illumination microscopy," *Optica* **3**, 667 (6 2016).

[16] van de Giessen, M., Angelo, J. P., and Gioux, S., "Real-time, profile-corrected single snapshot imaging of optical properties," *Biomedical Optics Express* **6**, 4051 (10 2015).

[17] Vervandier, J. and Gioux, S., "Single snapshot imaging of optical properties," *Biomedical Optics Express* **4**, 2938 (12 2013).

[18] Cuccia, D. J., Bevilacqua, F., Durkin, A. J., Ayers, F. R., and Tromberg, B. J., "Quantitation and mapping of tissue optical properties using modulated imaging," *Journal of Biomedical Optics* **14**(2), 024012 (2009).

[19] Angelo, J., Vargas, C. R., Lee, B. T., Bigio, I. J., and Gioux, S., "Ultrafast optical property map generation using lookup tables," *Journal of Biomedical Optics* **21**(11), 110501 (2016).

[20] "http://opensfdi.org/appsfdi/," (2021).

[21] Aguénounon, E., Smith, J. T., Al-Taher, M., Diana, M., Intes, X., and Gioux, S., "Real-time, wide-field and high-quality single snapshot imaging of optical properties with profile correction using deep learning," *Biomedical Optics Express* **11**(10), 5701 (2020).

[22] Schweiger, M. and Arridge, S., "The Toast++ software suite for forward and inverse modeling in optical tomography," *Journal of Biomedical Optics* **19**, 040801 (4 2014).

[23] Leino, A. A., Pulkkinen, A., and Tarvainen, T., "ValoMC: a Monte Carlo software and MATLAB toolbox for simulating light transport in biological tissue," *OSA Continuum* **2**, 957 (3 2019).

[24] Liu, Y., Jacques, S. L., Azimipour, M., Rogers, J. D., Pashaie, R., and Eliceiri, K. W., "OptogenSIM: a 3D Monte Carlo simulation platform for light delivery design in optogenetics," *Biomedical Optics Express* **6**, 4859 (12 2015).

[25] Cassidy, J., Nouri, A., Betz, V., and Lilge, L., "High-performance, robustly verified Monte Carlo simulation with FullMonte," *Journal of Biomedical Optics* **23**, 1 (8 2018).

[26] Dempsey, L. A., Persad, M., Powell, S., Chitnis, D., and Hebden, J. C., "Geometrically complex 3D-printed phantoms for diffuse optical imaging," *Biomedical Optics Express* **8**, 1754 (3 2017).

[27] Visentini-Scarzanella, M., Kawasaki, H., Furukawa, R., Bonino, M., Arolfo, S., Lo Secco, G., Arezzo, A., Menciassi, A., Dario, P., and Ciuti, G., "A structured light laser probe for gastrointestinal polyp size measurement: a preliminary comparative study," *Endoscopy International Open* **06**, E602–E609 (5 2018).

[28] "https://www.hexagonmi.com/products/structured-light-scanners/aicon-stereoscan-neo," (2 2021).

[29] "https://www.zivid.com/zivid-one-plus," (2 2021).

[30] Takeda, M. and Mutoh, K., "Fourier transform profilometry for the automatic measurement of 3-D object shapes," *Applied Optics* **22**(24), 3977 (1983).

[31] Liu, H., Lin, H., and Yao, L., "Calibration method for projector-camera-based telecentric fringe projection profilometry system," *Optics Express* **25**, 31492 (12 2017).

[32] Omidi, P., Yip, L. C., Wang, H., Diop, M., and Carson, J. J., "PhaseWare: Phase map retrieval for fringe projection profilometry and off-axis digital holographic interferometry," *SoftwareX* **13** (1 2021).

[33] Ribbens, B., "Projection Moiré profilometry simulation software for algorithm validation and setup optimalisation Active 3D thermography using projection profilometry View project PhairywinD View project," tech. rep. (2013).

[34] Ribbens, B., Jacobs, V., Dirckx, J., Vanlanduit, S., and Buytaert, J., "Projection Moire Profilometry Simulation Software for Algorithm Validation and Setup Optimisation," (2013).

[35] David A. Boas, Constantinos Pitris, N. R., [*HANDBOOK OF BIOMEDICAL OPTICS*], CRC Press (2011).

[36] Holmer, C., Lehmann, K. S., Wanken, J., Reissfelder, C., Roggan, A., Mueller, G., Buhr, H. J., and Ritz, J.-P., "Optical properties of adenocarcinoma and squamous cell carcinoma of the gastroesophageal junction," *Journal of Biomedical Optics* **12**(1), 014025 (2007).

[37] Erfanzadeh, M., Nandy, S., Kumavor, P. D., and Zhu, Q., "Low-cost compact multispectral spatial frequency domain imaging prototype for tissue characterization," *Biomedical Optics Express* **9**(11), 5503 (2018).